Journal Pre-proof

New dielectric/metal/dielectric electrode for organic photovoltaic cells using Cu:Al alloy as metal

L. Cattin, A. El Mahlali, M.A. Cherif, S. Touihri, Z. El Jouad, Y. Mouchaal, P. Blanchard, G. Louarn, H. Essaidi, M. Addou, A. Khelil, P. Torchio, J.C. Bernède

Please cite this article as: L. Cattin, A. El Mahlali, M.A. Cherif, S. Touihri, Z. El Jouad, Y. Mouchaal, P. Blanchard, G. Louarn, H. Essaidi, M. Addou, A. Khelil, P. Torchio, J.C. Bernède, New dielectric/ metal/dielectric electrode for organic photovoltaic cells using Cu:Al alloy as metal, *Journal of Alloys and Compounds* (2019), doi: https://doi.org/10.1016/j.jallcom.2019.152974.

This is a PDF file of an article that has undergone enhancements after acceptance, such as the addition of a cover page and metadata, and formatting for readability, but it is not yet the definitive version of record. This version will undergo additional copyediting, typesetting and review before it is published in its final form, but we are providing this version to give early visibility of the article. Please note that, during the production process, errors may be discovered which could affect the content, and all legal disclaimers that apply to the journal pertain.
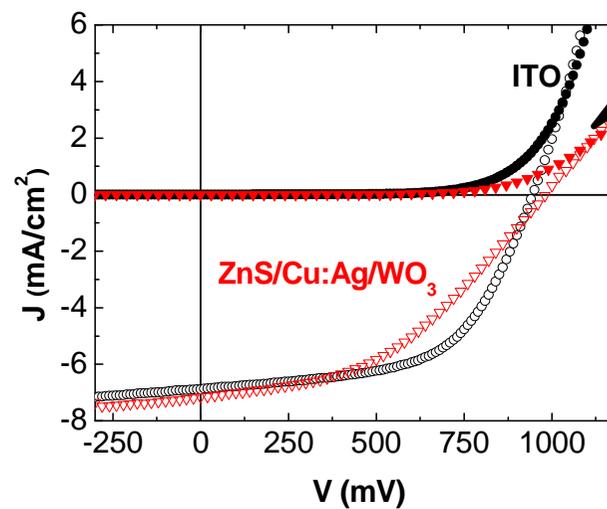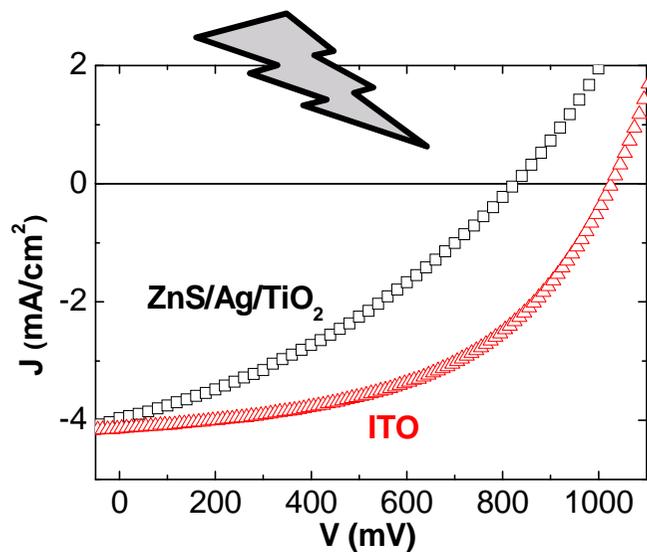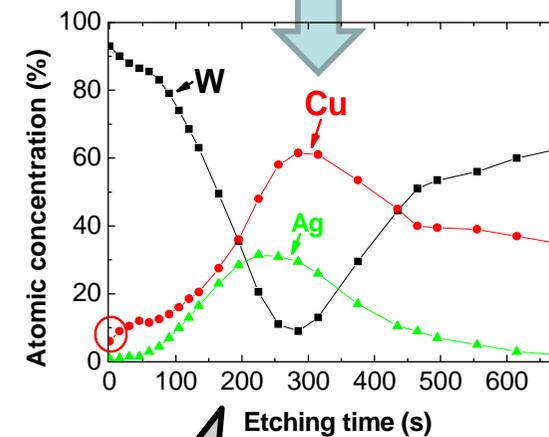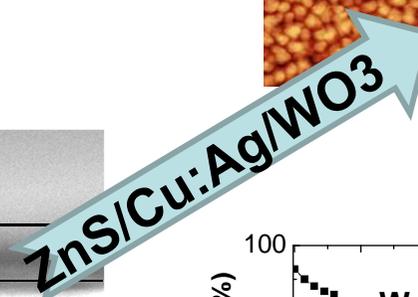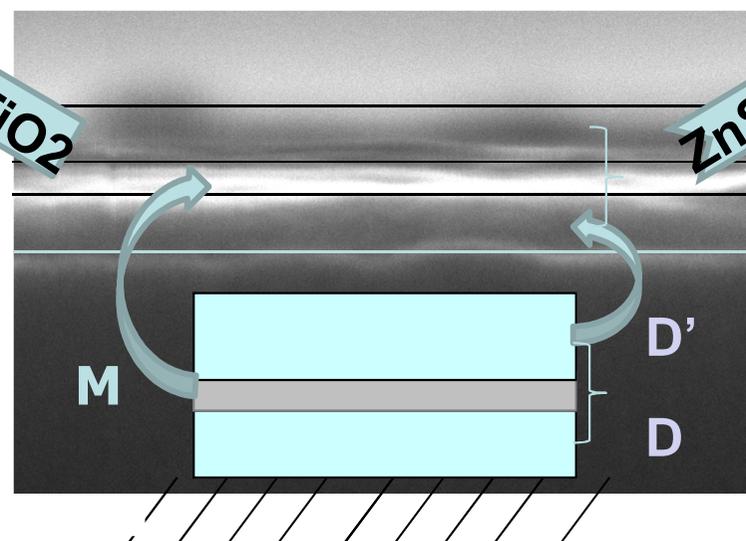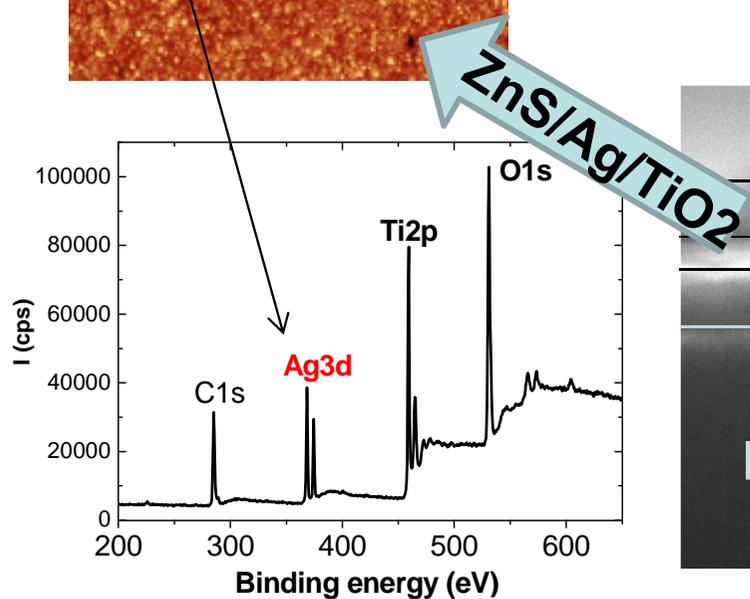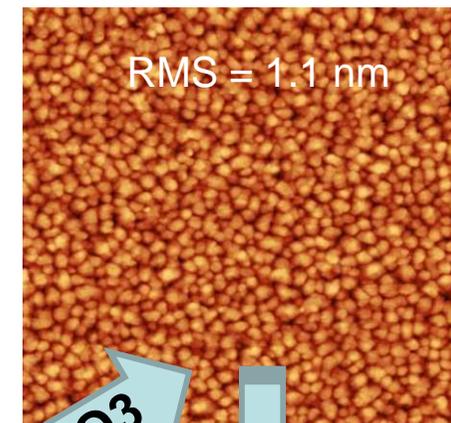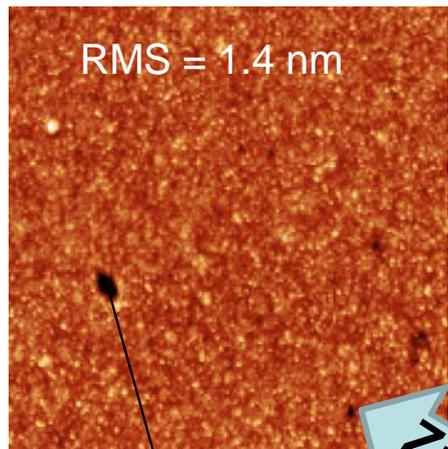
RMS = 1.4 nm

RMS = 1.1 nm

ZnS/Ag/TiO2

ZnS/Cu:Ag/WO3

O1s

Ti2p

Ag3d

C1s

I (cps)

Binding energy (eV)

M

D'

D

W

Cu

Ag

Atomic concentration (%)

Etching time (s)

ZnS/Ag/TiO₂

ITO

J (mA/cm²)

V (mV)

ITO

ZnS/Cu:Ag/WO₃

J (mA/cm²)

V (mV)

New Dielectric/Metal/Dielectric electrode for organic photovoltaic cells using Cu:Al alloy as metal.

L. Cattin[1], A. El Mahlali[1], M. A. Cherif[2,3], S. Touihri[3,7], Z. El Jouad[1,4], Y. Mouchaal[5,8], P. Blanchard[6], G. Louarn[1], H. Essaidi[3,6], M. Addou[4], A. Khelil[5], P. Torchio[2] and JC Bernède[7]

[1]Institut des Matériaux Jean Rouxel (IMN), CNRS-UMR 6502,Université de Nantes, 2 rue de la Houssinière, BP 32229, 44322 Nantes Cedex 3, France.
[2]Aix-Marseille Université, Institut Matériaux Microélectronique Nanosciences de Provence – IM2NP, CNRS-UMR 7334, Domaine Universitaire de Saint-Jérôme, 13 397 Marseille Cedex 20, France
[3]UPDS, Faculté des Sciences de Tunis, Université de Tunis El Manar, Tunis, Tunisia
[4]LMVR, FST, Université Abdelmalek Essaidi, Tanger, Ancienne Route de l'Aéroport, Km 10, Ziaten, BP: 416, Morocco
[5]Université d'Oran 1 - Ahmed Ben Bella, LPCMME, BP 1524 ELM Naouer 31000 Oran, Algeria
[6]MOLTECH-Anjou, UMR 6200, UNIV Angers, CNRS, 2 bd Lavoisier, 49045 ANGERS Cedex, France.
[7]MOLTECH-Anjou, CNRS-UMR 6200, Université de Nantes, 2 rue de la Houssinière, BP 92208, Nantes, F-44322, France
[8]Faculté des Sciences Exactes, Université de Mascara, B.P. 305, 29000 Mascara, Algeria

Abstract
Given the rapidly increasing demand for flexible and inexpensive optoelectronic devices, it is necessary to find a substitute for ITO (Indium Tin Oxide). Among the considered alternatives, we have chosen in the present work Dielectric/Metal/Dielectric (D/M/D) trilayer structures deposited under vacuum. In these D/M/D structures, when Ag is the metal, highly performing and stable Transparent Conductive Electrodes (TCEs) are obtained. When Ag is replaced by Cu, which is far less expensive, results are not similar due to the tendency of Cu to diffuse into the transition metal oxides. Therefore we improve the stability of the new TCEs by using the Cu alloy Cu:Ag in $ZnS/M/WO_3$ structures. The best results were obtained when M = Cu:Ag (16 nm)/Ag (1 nm). Flexible and quite stable TCEs were obtained.
These new TCEs are conductive and transparent with a figure of merit of 6.5 x $10^{-3}\Omega^{-1}$ and a quite small Root Mean Squared Roughnessis (RMS = 1.1 nm). Therefore, they were introduced as anode in organic photovoltaic cells (OPVs). In the same time, $ZnS/Ag/TiO_2$ TCE were probed. These $ZnS/Ag/TiO_2$ structures were transparent and conductive with optical and electrical performances similar to those of ITO, but, when used as anode, the OPVs performances were limited by the presence of Ag at the surface of the structures. In the other hand, the results obtained with $ZnS/M/WO_3$ structures were very promising with an open circuit voltage, Voc, and a short circuit current, Jsc, whose values are slightly higher than those obtained with ITO. Nevertheless the fill factor FF is sensibly smaller, which is attributed to the presence of some Cu at the surface of the electrode.

Corresponding author: J. C. Bernède E-mail: jean-christian.bernede@univ-nantes.fr

1. Introduction

Flexible organic photovoltaic cells (OPVs) attract high interest for solar energy. They are based on organic films sandwiched between two electrodes, one of them being transparent and conductive [1, 2]. ITO (Indium Tin Oxide) is the TCE the most often used because it presents many advantages such as excellent optical properties and good conductivity. However, it has also some disadvantages such as indium scarcity, the use of aggressive techniques of deposits for organic materials and brittleness [3]. Therefore, an urgent need for alternatives to ITO by new Transparent Conductive Electrode (TCE) arises. This TCE must have similar electrical and optical performance as ITO. The elements constituting should be abundant and neutral environmental and integrate into the framework of sustainable development. The techniques used for its deposition should be as gentle as possible. The flexibility of the TCE and adhesion must be compatible with the use of a plastic substrate. Several solutions have been explored to replace ITO [4, 5]. Among them, multilayer structures of Dielectric / Metal / Dielectric (D/M/D) [6-8] are very promising. In the context of research on organic compounds, many works are devoted to wet deposition, because they appear inexpensive [9]. However, dry process under vacuum allows stacking many layers without difficulty. These layers are pure and their properties are reproducible which reduces the cost of a large-scale production [10]. Thus, the present manuscript is dedicated to the realization of high-performance and stable D/M/D structures using a Cu alloy as metal. After characterization, these new TCEs are introduced in organic photovoltaic cells (OPVs), which are based on planar heterojunctions (PHJ), the whole devices being deposited under vacuum.

In addition to confirmation of the Ag's effectiveness as metal in $ZnS/Ag/TiO_2$ structures through the use of such electrodes as cathodes in OPVs, our investigations are focused on Cu that is far cheaper than Ag. However, Cu has a high tendency to diffuse in transition metal oxides [11]. We have already shown that using Cu alloys such as Cu:Ni or Cu:Al allows temperate significantly this parasitic effect [12, 13]. Nevertheless, some difficulties are still present. For instance in the case of the Cu:Ni alloy, it is difficult to increase the D/Cu/D structure stability through an increase of the Ni concentration by simple evaporation, its melting point being far higher than that of Cu [12]. On the other hand, in the case of Al we have shown that the stability of the electrodes are significantly improved through the introduction of a thin Ag layer (2 nm) between the alloy Cu:Al and the top dielectric layer. Actually, this ultra-thin film permits to improve the stability of the alloy by diffusing it in its volume [13]. Therefore, in the present work we focus our interest on Cu:Ag alloy. After raising at least partially this technological obstacle, the new electrodes were introduced in OPVs. It must be noted the focus of this work is dedicated to ITO free electrodes. So the cells realized with these electrodes were only to show the possible utilisation of these electrodes and not to compete with the best cells today produced. That is why we used a classical already known multilayers planar hetero-junction structure based on Boron subphthalocyanine chloride/fullerene (SubPc/C_{60}) junction.

2

2. Description of approach and techniques

2.1 New transparent conductive electrode deposition and characterization techniques

The substrates used during this work were either soda-lime glass or poly(ethylene terephthalate) (PET). TCE structures were deposited on glass or on PET (150 μm thick). The cleaning of the substrates and the deposition process are described in supporting information S1 [14]. Multilayer structures D/M/D were deposited without breaking the vacuum.

After deposition the structures were systematically submitted to optical and electrical characterizations. Optical and electrical characterization techniques are reported in S2.

From optical and electrical measurements, in order to determinate the best compromise "Conductivity-Transmission", we calculate the figure of merit (Φ_M) proposed by Haack using the empiric formulae [15]:

$$\Phi_M = T^{10}/\sigma_{sh}.$$

where T is transmission and σ_{sh} sheet resistance,

Thanks to this formula it is possible to compare the "opto-electrical" performances of the different electrodes.

The surface morphology of the D/M/D multilayer structures was studied with a field emission scanning electron microscope (SEM, JEOL F-7600) and an atomic force microscope. (Supporting information S3).

The scotch tape method [16] was used to estimate the adhesion of the structures to the substrate (See S4.1). The flexibility of the D/M/D structures was studied using a laboratory made bending test system (See S4.2). The depth profile of the structures was studied by recording successive XPS spectra obtained after argon ion etching for short periods (S4.3).

2.2 Realization and characterization techniques of organic photovoltaic cells using new TCE.

D/M/D multilayer structures were used as electrodes in OPVs to test their potential. To this end, we made OPVs using the planar heterojunction geometry, namely [17]:

Glass substrate/TCE anode/CuI/SubPc/C_{60}/BCP/Al, in the case of classical OPVs, and Glass substrate/TCE cathode/BCP/C_{60}/SubPc/Al, in the case of inverted OPVs.

In these structures, CuI is the hole transporting layer (HTL) [17], BCP is the exciton blocking layer (EBL) [18], Al the cathode (classical cells) or the anode (inverted cells), while SubPc is the electron donor (ED) and C_{60} is the electron acceptor (EA) of the planar heterojunction of the OPV. With regard to the transparent electrode, we used our new TCEs, and also ITO in reference OPVs. The ITO thin film was 100 nm-thick and its sheet resistance was 20 Ω/sq, in the case of glass substrates, and 100 Ω/sq in the case of PET substrates.

The electrical characterization of the OPVs was performed with an I-V tester, in the dark and under sun global AM 1.5 simulated solar illumination. J-V curves under illumination were used to calculate the series resistance (Rs) and the shunt resistance (Rsh) of OPVs to investigate the charge carrier collection. The series resistance, Rs, of OPVs is equal to the reciprocal of J-V curve slope at Voc, while the shunt resistance, Rsh, is equal to the reciprocal of J-V curve slope at Jsc.

3

3. Results and discussion

3.1 D/M/D multilayer modeling

Before any experimentation we carried out optical modeling, which aims to model and simulate the optical properties of D/M/D multilayered electrodes and of complete solar cells. The ability to numerically optimize the opto-geometrical parameters of the new TCE, as well as the intrinsic absorption inside the active layer of the devices, allows guiding the experimental studies by providing the values of the optimal thicknesses of the oxide layers of the TCE and of the layers of whole devices [19]. For that, the optical constants of organic and inorganic materials, constituents of the solar cells, were incorporated in our Transfer Matrix Method (TMM) numerical model [20, 21, 22]. The thicknesses of the multilayer can then be optimized by taking into account the interference phenomena induced by all interfaces, in order to locate the maximum power electromagnetic dissipated in the excitons generating active layer.

The efficiency of this optical modeling has been proved through its application to $ZnS/Ag/TiO_2$ based-TCE (ZAT-TCE) [23]. As an example, the Figure 1 presents the compared data of optical properties from a simulated and fabricated ZAT-TCE. A broad [365-695] nm transmission range where T is above 80% is revealed, while the sheet resistance is measured below 10 Ω/sq. Optical results are in good agreement between theory and experience. The small observed difference could probably be due to the morphology of Ag, which is not fully homogeneous but presents some nano-islands (for this 10 nm-thick layer). This can result in enhanced absorbance due to plasmonic resonances, involving a decreased transmittance for the manufactured electrodes compared to the theoretical ones (heterogeneities in morphology are not taken into consideration by TMM simulation) [24].
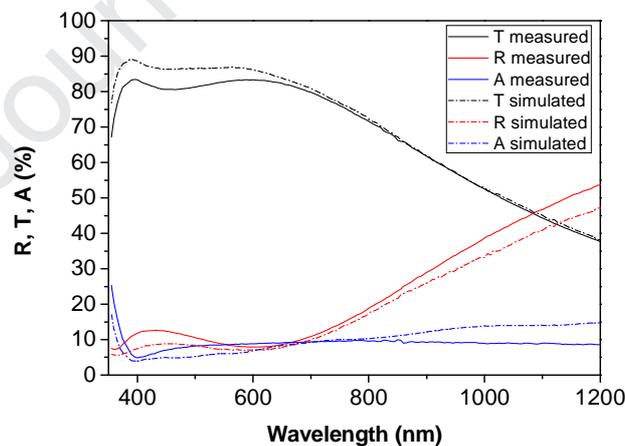

Figure 1: Comparison between simulated and measured values of transmittance (T), reflectance (R) and absorbance (A) for a ZnS (35 nm) / Ag (10 nm) / TiO_2 (25 nm) electrode

Similar theoretical-experimental dialectic was used to optimize the others D/M/D structures. For instance, it results that the optimum bottom layer thickness was 50 nm, 45 nm and 35 nm for ZnS, MoO_3 and WO_3 respectively, while it was 45 nm, 37.5 nm and 20 nm for the corresponding top layer [21-24]. When the metal is Ag, the optimum thickness is around 11-13 nm. Below this thickness the Ag film is discontinuous involving that the structures are

4

insulating, beyond this thickness their reflectance increases and therefore their Figure of merit decreases.

Thanks to this figure of merit, Φ_M, it is possible to compare the « opto-electrical » performances of the different electrodes. For instance the averaged Φ_M value of the $ZnS/Ag/TiO_2$ structures presented above is around $\Phi_M = 15 \times 10^{-3}\ \Omega^{-1}$, which is of the same order of magnitude than that of ITO [7].

Similar results were obtained with $WO_3/M/WO_3$ and $ZnS/M/WO_3$ structures. After this optical modeling, which allows estimating the optimum thicknesses of the dielectric layers, that of the metal being also strongly dependent of the required conductivity, we proceeded to the experimental study of D/Cu/D structure using Cu:Ag alloy as metal layer.

3.2 D/Cu/D multilayer characterizations

As evocated in the introduction, it should be better to substitute Cu to Ag that is quite expensive. Nevertheless it is not so easy to obtain performing D/M/D multilayer with Cu as metal because, if the electrical properties of Cu are nearly similar to that of Ag, its diffusion coefficient is significantly higher, which makes difficult to obtain stable D/Cu/D structures. For instance, in the case of $MoO_3/Cu/MoO_3$ structures, we have shown that it is necessary to insert ultra thin Al layers (1 nm-thick) between Cu and MoO_3 to obtain conductive structures [11]. One possibility to improve the stability of the Cu-based structure is to substitute a Cu alloy to Cu pure metal. Thus, we have proved that using Cu:Ni alloy permits to increase the stability of the D/Cu/D structures [12]. Moreover we have shown that better results are obtained when WO_3 is substituted to MoO_3, due to the higher density of the WO_3 layers. The $WO_3/Cu:Ni/WO_3$ structures are far more stable than the $MoO_3/Cu/MoO_3$ structures. Nevertheless, at the percolation thickness of the Cu:Ni layer, *i.e.* when the structure commutes from the insulating to the conductive state, which corresponds to its maximum transmission, the sheet resistance of the structure increases slowly, but continuously, with time (Figure 2). Moreover, as shown by XPS profiles, there is some Cu accumulation at the surface of the structures which has a negative effect on the performances of the organic photovoltaic cells using these structures as anodes [12]. Actually, we were unable to overpass an atomic concentration of 1% of nickel in the Cu metal alloy due to the higher melting temperature of Ni, our deposition technique using simple Joule effect for the evaporation. Therefore, in order to persist in the use of the simple deposition technique based on Joule effect heating, we used Cu:Al alloy in a second attempt, Al being far easier than Ni to evaporate.

Thus, in a recent study [13] we have shown that the use of Cu:Al allows improving the stability of the $WO_3/M/WO_3$ structures by comparison with those using Cu alone. Moreover, the insertion of a thin (2 nm) Ag layer between Cu:Al and the WO_3 bottom layer permits to obtain far more stable TCEs. Furthermore there is less Cu accumulation at the surface of the electrode which leads to more performing OPVs. Unfortunately, here also the stability of the sheet resistance is not as high as that of structures using Ag as metal [25] (Figure 2). To try to understand this behaviour we had performed XPS studies to examine the profile of the multilayer structures. Surprisingly, the XPS profile of the $WO_3/Ag/Cu:Al/WO_3$ structures showed that Ag has diffused all along the thickness of the Cu:Al layer. It means that Ag diffuses spontaneously into Cu to form a quite stable alloy. It was concluded that the formation of Cu:Ag alloy has a positive effect on the stability of the structures.
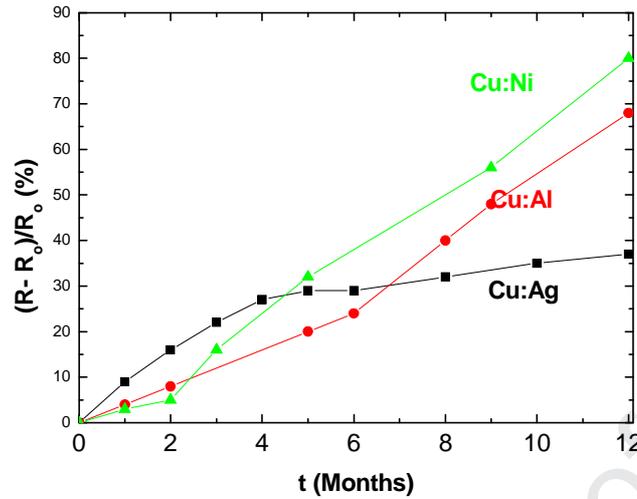
5

Figure 2: Evolution with time of the sheet resistance of
$WO_3/Cu:Ni/WO_3$ (▲), $WO_3/Cu:Al/Ag/WO_3$ (●) and $ZnS/Cu:Ag/Ag/WO_3$ (■) structures.

As a matter of fact, it must be noted that Ag and Cu have large miscibility and a relative atomic size difference of only 12%, which allows this miscibility and eutectic possible formation [26]. The maximum solubility of Ag in Cu is 7.47 at.%, which may possible the Ag diffusion in the present structures, the maximum of Ag in the profile being 4 at.% [13]. Therefore, since Ag forms spontaneously a stable alloy with Cu, we decided to work with the alloy Cu:Ag instead of using Cu:Al and Ag. The atomic concentration of Ag in the starting alloy was 5 at.%. Moreover, since the Cu diffusion into ZnS is smaller than that into transition metal oxides, we chose ZnS as bottom dielectric layer [27], while we kept WO_3 as top dielectric layer, due to its high efficiency as HTL in OPVs. Finally, the different structures studied were as follows:

$ZnS/Cu:Ag(x$ nm$)/Ag$ (y nm$)/WO_3$(ZCAW), with 14 nm$< x < 19$ nm and $0 < y < 2$ nm. The optimum thicknesses of ZnS (45 nm) and WO_3 (20) have been estimated theoretically as discussed above.

Cu:Ag (x nm)	T (%) maximum	T (%) average*	Rsh (Ω/sq)	Φ (Ω^{-1}) maximum	Φ (Ω^{-1}) average*
14	79.5	66.4	63	0.0016	2.6 x10^{-4}
15	83.1	71.6	33	0.0047	0.0011
16	85.2	76.2	31	0.0065	00021
17.5	80.8	71.5	27	0.0044	0.0013
18	80.6	71.3	21	0.0055	0,0016
19	80.3	71.0	19	0.0058	0,0017

* Average value between 400 and 700nm.

Table 1: Variation of the main parameters of the ZnS (45 nm)/Cu:Ag (x nm)/Ag (1 nm)/WO$_3$ (20 nm) multilayer structures with the thickness x of Cu:Al layer, the Ag layer thickness being fixed at y = 1 nm.

6
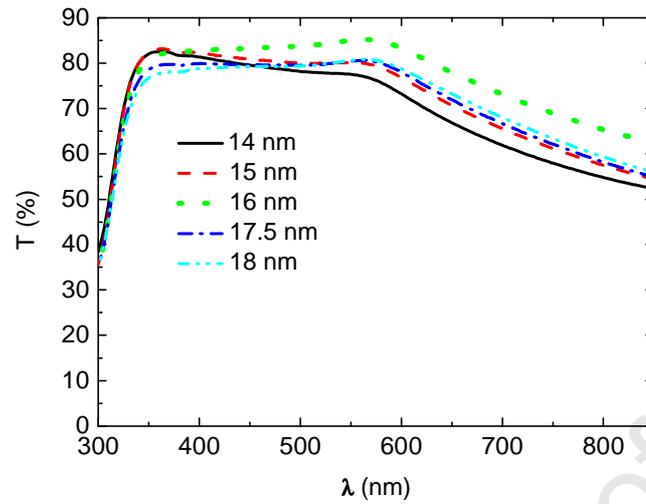
Figure 3: Variation of the light transmission of the
ZnS (45 nm)/Cu:Ag (x nm)/ Ag (1 nm)/WO$_3$ (20 nm) structures with different thicknesses for the Cu:Ag layer.

The evolution of the transmission spectra of the structures with the Cu:Ag layer thickness, that of the ultra-thin Ag layer being y = 1 nm, is shown in Figure 3 and is summarized in Table 1. The maximum of transmission, T_{Max} = 85.2% at λ_{Max} = 565 nm is obtained when the Cu:Ag layer thickness is 16 nm. Its averaged transmission is 76.2% between 400 nm and 700nm.

Ag (y nm)	Cu:Ag (x nm)	T (%) maximum	T (%) average*	Rsh (Ω/sq)	ΦΦΦΩ⁻¹) maximum	ΦΦΦΩ⁻¹) average*
0	17	85.9	78.1	36	0.0060	0.0023
1	16	85.2	76.2	31	0.0065	0.0021
2	15	83.9	71.9	30	0.0057	0.0012

Table 2: Variation of the main parameters of the ZnS (45 nm)/Cu:Ag (x nm)/Ag (y nm)/WO$_3$ (20 nm) multilayer structures, y, the Ag thickness and x the Cu:Ag thickness being used as parameters, while the sum x+y is constant: 17 nm.

After optimization of the Cu:Ag film thickness, x = 16 nm, with y = 1 nm of Ag, we have checked the influence of the thickness of the y, while we kept the total metal thickness constant, x + Y = 17 nm. The results obtained are presented in Table 2. It can be seen that that fairly close performances are obtained. Nevertheless, the presence of an ultra-thin Ag layer permits improving TCE stability [13]. Therefore we choose to work with the following structures ZnS (45 nm)/Cu:Ag (16 nm)/Ag (1 nm)/WO$_3$(20 nm), since this structure gives the highest figure of merit, Φ_M = 6.5 x $10^{-3}\Omega^{-1}$. A so thin thickness value, y = 1 nm, corresponds to an average value and not to a real continuous film thick of 1 nm. Nevertheless the knowledge of this averaged thickness allows to estimate the quantity of Ag present in the alloy Cu:Ag, since Ag diffuse into the Cu layer after deposition.

7

As usual in this kind of D/M/D structures, the transmission of light increases with the metal film thickness up to a crtical optimum value, here 16 nm, then, beyond this thickness it starts to decrease. It must be noted that this optimum thickness corresponds to the commutation of the resistance of the film from insulating to conducting state. Actually this critical thickness corresponds to the percolation of the metal layer, which becomes homogeneous. Below this thickness the metal film is not continuous and, not only it is insulating, but the heterogeneities present in the discontinuous film induces light diffusion. Beyond this thickness the sheet resistance of the structures decreases slowly, but the light transmission decreases sensibly and the optimum figure of merit is obtained for the critical metal layer thickness.

A surface visualization of a $ZnS/Cu:Ag/Ag/WO_3$ structure is visible in Figure 4a. This surface is homogeneous, for higher magnification, its granular morphology is clearly visible (inset in Figure 4a). In Figure 4b we show the cross-section image, in the backscattering mode, of a $ZnS/Cu:Ag/Ag/WO_3$ structure. It is known that this mode allows discriminating between the domains of different composition, since the brilliance of the image increases with the atomic weight of the element present in this domain. In Figure 4b, two grey domains enclose a white stripe. Since the averaged molecular weight of the metals is higher than that of the dielectrics, the central stripe corresponds to the metal layer while the two grey domains correspond to ZnS (left) and WO_3 (right).
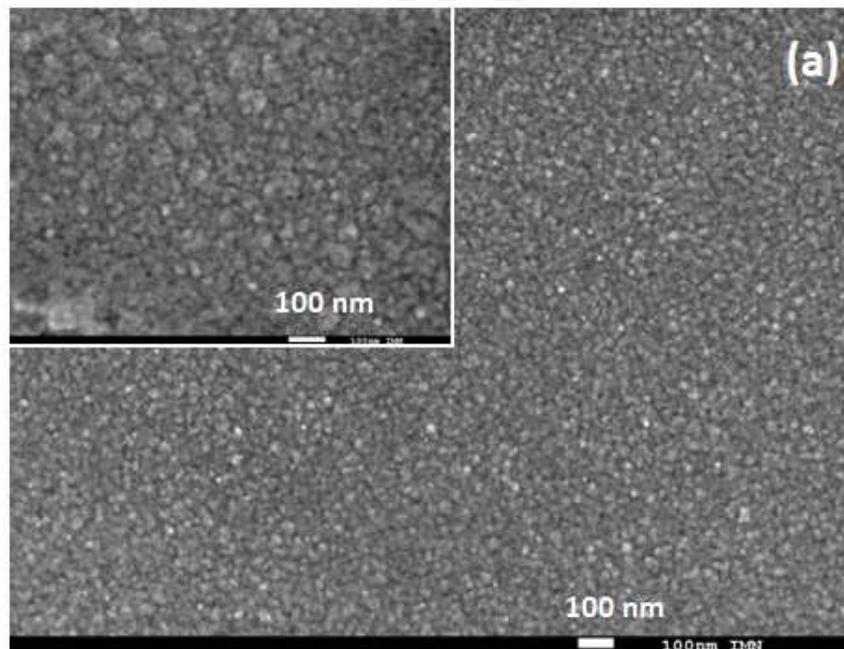

Figure 4: a-Surface visualization of a ZnS(45 nm)/ Cu:Ag (16 nm)/ Ag (1 nm)/WO₃ (20 nm) multilayer structure; inset: same film at higher magnification.
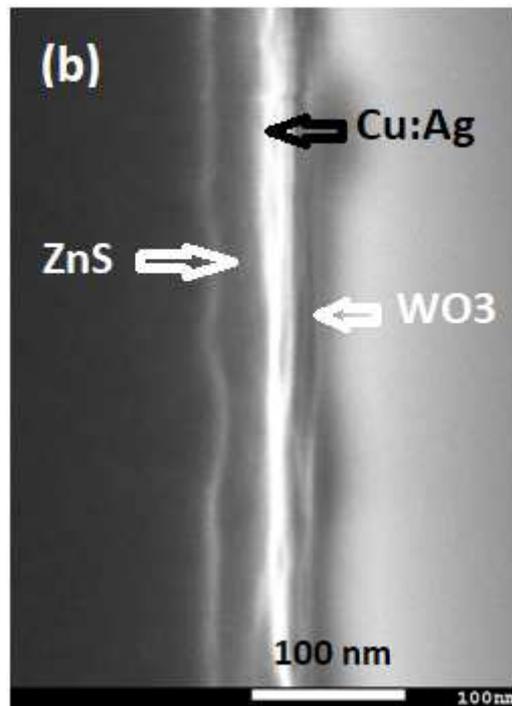
Figure: b- Cross section visualization in the backscattering mode of a ZnS(45 nm)/ Cu:Ag (16 nm)/ Ag (1 nm)/WO$_3$ (20 nm) structure.
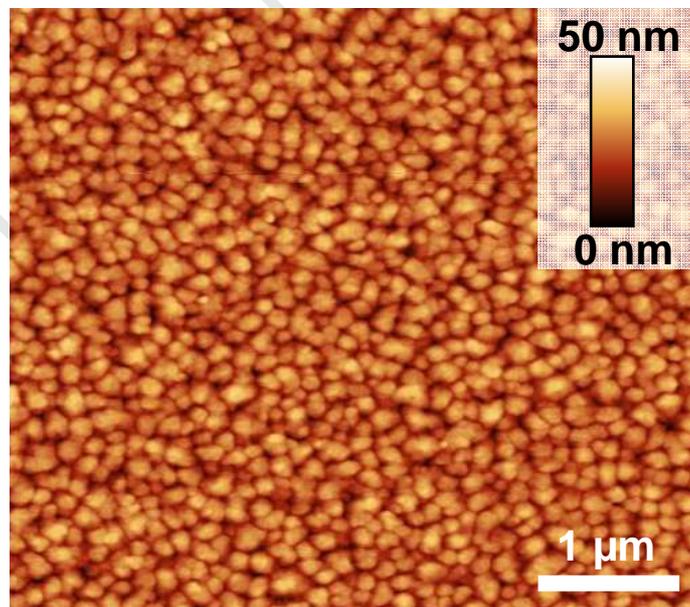
Figure 5: AFM image of the surface of a ZnS(45 nm)/ Cu:Al (16 nm)/ Ag (1 nm)/WO$_3$ (20 nm) multilayer structure.

An AFM image of such TCE is presented in Figure 5. It can be seen that it appears quite homogeneous. Its Root Mean Squared Roughnessis RMS = 1.1 nm. This small value is encouraging for organic optoelectronic devices realization, since too high roughness could induce leakage currents.

9

Samples were also deposited onto PET flexible substrates in order to check their flexibility (S4.2). The films were submitted to inner and outer bending, for a bending radius of 6 mm and a bending frequency of 1 Hz, it can be seen in Table 3 that the variation of the sheet resistance is negligible for the ZnS/Cu:Ag/Ag/WO$_3$ structures while it is not the case for ITO,

Number of cycles		0	1	5	10	50	500	1000	2000
	Inner bending	0	0	0	0	0	0	0	0
$\Delta R/R_o$(%)	Outer bending	0	0	0	0	0	0.5	1	2
	ITO (outer bending)	0	2	4	8	13	19	25	29

Table 3: Resistance evolution after outer bending and inner bending as a function of the number of bending cycles for PET/ZnS(40 nm)/ Cu:Al (16 nm)/ Ag (1 nm)/WO$_3$ (35 nm) and PET/ITO structures.

About the adhesion of the structures using Cu:Al as metal, the structures pass the tape test (S4.1) without difficulty, the films are not at all removed from the substrate. The electrical resistance of the structure is not modified by the test.

In order to check the composition of the metal alloy, we have estimated the composition of a film thick of 200 nm by microprobe analysis. The atomic concentrations obtained are 95 at% of Cu and 5 at% of Ag, which corresponds to the concentration of the alloy source (bulk alloy).
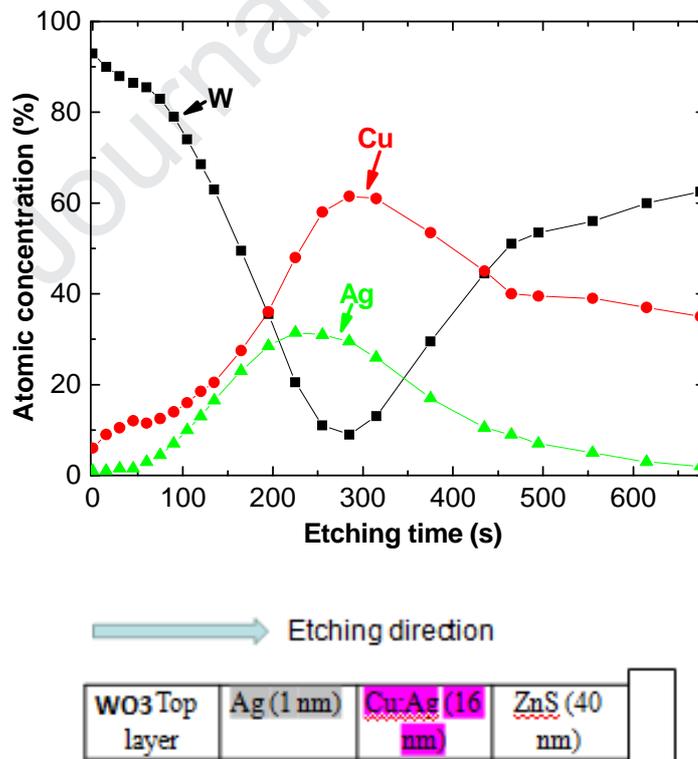

Figure 6: XPS profiles of Glass/ZnS (45 nm)/Cu:Ag (16 nm)/Ag (1 nm)/WO$_3$ (20 nm) and typical structural diagram of a structure.

10

We have also checked the profiles of concentration of the different atoms present in the structures. A typical profile of a $ZnS/Cu:Ag/Ag/WO_3$ structure is shown in Figure 6.

It can be seen that the three stacked layers, $ZnS/Cu:Ag/WO_3$ are clearly visible, which confirms that the top ultra-thin layer of Ag has diffused into the Cu layer, even if a small "memory" effect is present as shown by the fact that the Ag concentration peak is slightly shifted towards the surface of the structure. The atomic concentration of Cu at the surface of the structure, 5 at.%, is far smaller than that obtained with others alloys probed [12, 13]. Nevertheless, while it can be seen that the Ag atomic concentration tends towards zero when the etching time increases, that of Cu only decreases slowly. It corresponds probably to an artifact due to the etching process, which buried Cu atoms. Such parasitic effect testifies that if the diffusion of Cu is significantly decreased it is not completely blocked, which explains the slow evolution of the sample resistance over time (Figure 2).

However, as shown in figure 2, the Cu:Ag alloy is the more stable among the three alloys probed. Therefore, as a conclusion of the characterization of the new D/M/D' structures, it can be said that the new TCEs present the requested properties to be used as electrode in optoelectronic devices.

3.3 Organic solar cells with new transparent electrodes

After the characterization of the $ZnS/Ag/TiO_2$ and $ZnS/Cu:Ag/Ag/WO_3$ structures we have introduced these TCE in inverted and classical OPVs for the former structure and in classical OPVs for the latter structure. It is well known that a good band matching at the organic material/electrode interfaces is necessary for efficient carrier collection. Usually, a high work function (Φ_M) material is introduced on the anode side to obtain performing hole collection and one with a low Φ_M at the cathode side for efficient electron collection. Fortunately, WO_3 is well known as very efficient hole transporting layer (HTL) on the anode side, while TiO_2 is known as good electron transporting layer (ETL) on the cathode side, which makes that our D/Ag/D structures should be easily used as anode, in the case of WO_3 as top dielectric and as cathode, in the case of TiO_2. Nevertheless, we have already shown that, if these HTL and ETL layers are efficient, it is possible to optimize the performance of the OPVs by covering these layers with a thin layer of CuI for the HTL [28] and a layer of BCP for the ETL.

In order to compare easily the performances of our new TCEs to that of ITO, we used a very simple PHJ-OPV, based on the heterojunction $SubPc/C_{60}$ as couple ED/EA.

The first OPVs probed were inverted cells with the configuration:

Substrate/Cathode/BCP (9 nm)/C_{60}(35 nm)/SubPc (16 nm)/MoO_3 (7 nm)/Al, the cathode being either $ZnS/Ag/TiO_2$ or ITO. The thicknesses of the different layers were optimized in earlier studies [29].

Typical results are given in Figure 7 and Table 4.
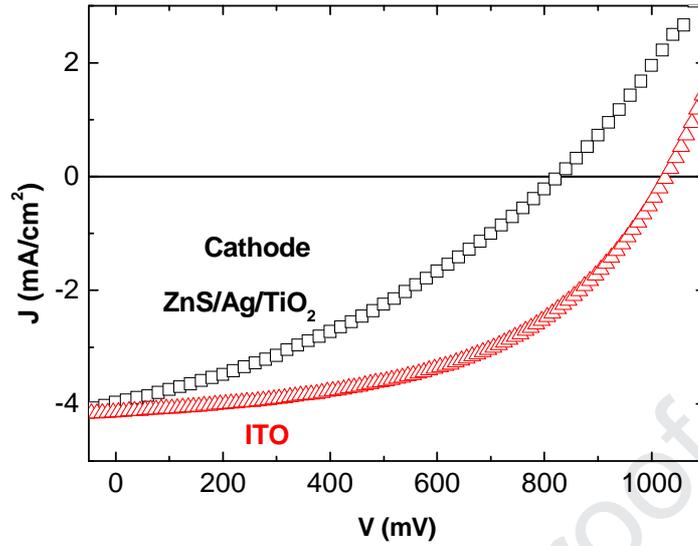
11

Figure 7: J-V characteristics of inverted OPVs (Cathode/BCP/C_{60}/SubPc/MoO$_3$/Al) with ZnS/Ag/TiO$_2$ (□) or ITO (▲) as cathode.

It can be seen that the efficiency obtained with the ZnS/Ag/TiO$_2$ cathode is smaller than that obtained with ITO. This difference originates mainly from Voc and FF values. They can be related to the difference of shunt resistance values, actually, Rsh = 1300 Ω for ITO and only 130 Ω for ZnS/Ag/TiO$_2$ (ZAT-TCE).

Cathode	Voc (V)	Jsc (mA/cm^2)	FF (%)	η (%)	Rs (Ω)	Rsh (Ω)
ITO	1.03	4.22	50	2.14	25	1300
ZnS/Ag/TiO$_2$	0.83	3.96	34	1.13	52	130

Table 4: Comparison of the parameters of the OPVs with ZnS/Ag/TiO$_2$ or ITO as cathode.

The sheet resistance of ZAT-TCE being only σ_{sq}= 10 Ω/sq, i.e. smaller than that of the ITO used in the present work (σ_{sh} = 20 Ω/sq), such difference in the Rsh values cannot be attributed to σ_{sq}. The small Rsh value, can originate from a too large RMS value of the bottom electrode, because a too large roughness can induce leakage currents. Therefore, we proceeded to an AFM study. A typical AFM image is shown in figure 8. The surface of the ZAT-TCE is highly homogeneous with a RMS of 1.4 nm. Only small scarce holes are visible in the TCE. Such small RMS cannot justify the small Rsh value.

12
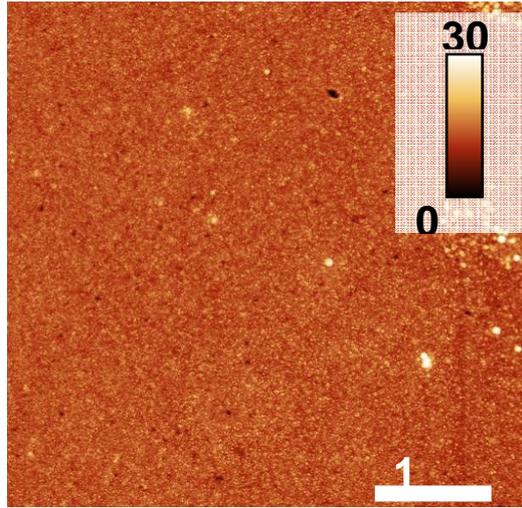
Figure 8: AFM image of the surface of ZnS/Ag/TiO$_2$

On the other hand, since in the case of classical OPVs, we have already shown that the optimum thickness of SubPc is 20 nm and not 16 nm as in the case of inverted OPVs [28], it is likely that Rsh of the classical OPVs is higher than that of inverted OPV. Therefore, as it has been shown that any metal with small work function, such as Al, can be used as anode in OPVs when it is covered by a MoO$_3$ layer [30], we have used ZnS/Ag/TiO$_2$/MoO$_3$ as anode in Anode/SubPc/C$_{60}$/BCP/Al OPVs. Typical results are shown in Figure 9. With ZnS/Ag/TiO$_2$ we obtained Voc = 0.70 V, Jsc = 4.34 mA/cm^2, FF = 52% and η = 1.56 %, Rs = 50 Ω, Rsh = 1000 Ω while with ITO we had Voc = 0.84 V, Jsc = 5.29 mA/cm^2, FF = 56% and η = 2.50%, Rs = 20 Ω, Rsh = 1050 Ω. Here, even if with 20 nm of SubPc the Rsh value measured with the ZAT anode is of the same order of magnitude than that obtained with ITO, the device efficiency is smaller. Actually, Voc and Jsc are significantly smaller than the corresponding values obtained with ITO anode.
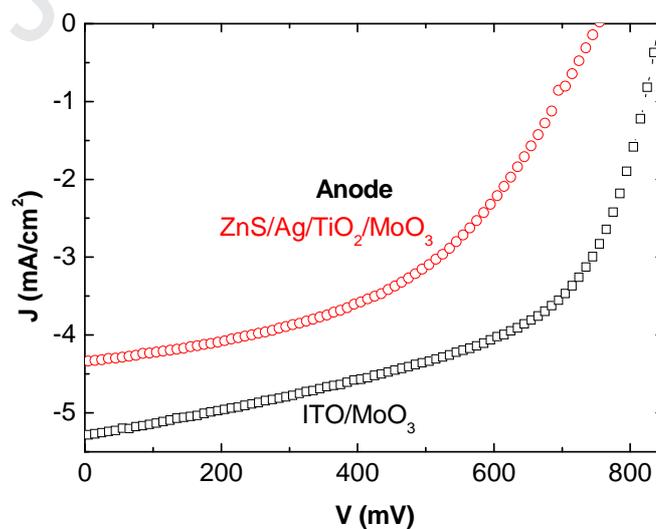
Figure 9: J-V characteristics of classical OPVs (Anode/MoO$_3$/SubPc/C$_{60}$/BCP/Al) with ITO (□) or ZnS/Ag/TiO$_2$ (○) as anode

13

In order to understand the decreases of the parameters of the OPVs using ZAT TCE, after the AFM study we proceeded to a surface analysis by XPS. The survey spectrum obtained is shown in Figure 10. It can be seen that if, as expected, Ti and O are detected, Ag is also present at the surface of the ZAT-TCE, while Zn is not.
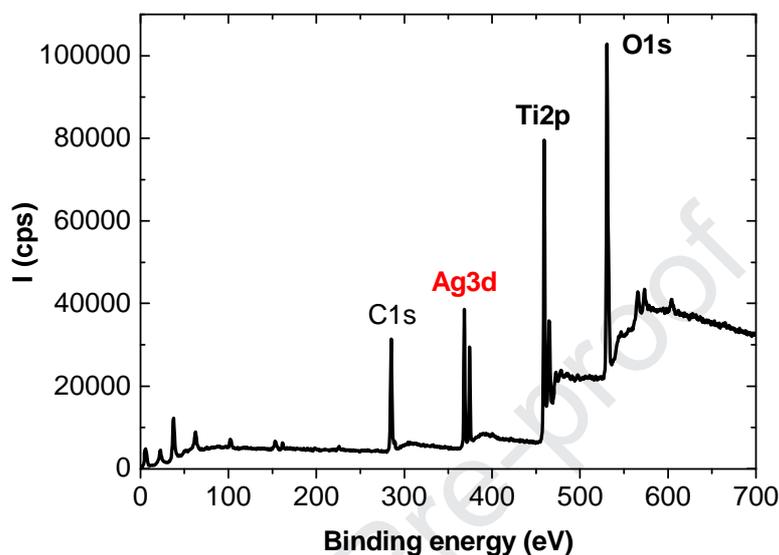

Figure 10: XPS survey spectrum of a ZnS/Ag/TiO$_2$ structure.

More precisely, the relative atomic concentration of Ag is 14% for 86 at.% of Ti. The presence of Ag randomly distributed to the electrode surface may explain the decrease of cell parameters. The binding energy of the peak Ag3d being poorly sensible to Ag oxidation state, it is difficult to determine precisely the oxidation state of Ag. Nevertheless the samples being stored in room air before to be used as electrode, the surface atom of Ag must be, at least partially, oxidized. It means that the work function of Ag present at the surface of the electrode is situated between 4.5 eV and 5 eV. This value is too high to give a good cathode, but too small to give a good anode. That can explain the limitation of the OPVs using ZAT electrodes. About the small value of Rsh in Table 4, as shown by the presence of Ag at the surface of ZnS/Ag/TiO$_2$ structures, if the diffusion of Ag atoms is smaller than that of Cu, it is not negligible. It was already shown that, in the case of silver/semiconductor/metal devices, during J-V characteristics scans, Ag can diffuse from the electrode to the semiconductor, forming a conductive filament in the semiconductor [31]. Therefore, the surface concentration of Ag atoms being as high as 14%, the ability of Ag to diffuse makes it possible for leak paths to appear through the thin organic layer, inducing a quite high saturation current and a small Rsh. In the future, it will be possible to avoid the presence of Ag at the surface of the structure by increasing the thickness of the TiO$_2$ film.

After showing that ZnS/Ag/TiO$_2$ structures can successfully be used as cathode or anode in OPVs, we probed ZnS/Cu:Ag/Ag/WO$_3$ structures as anode in OPVs.

Here the OPVs were as follows: Anode/CuI (1.5 nm) /SubPc (20 nm)/C$_{60}$ (35 nm)/BCP (9 nm)/Al, the results obtained are presented in Figure 11 and Table 5.
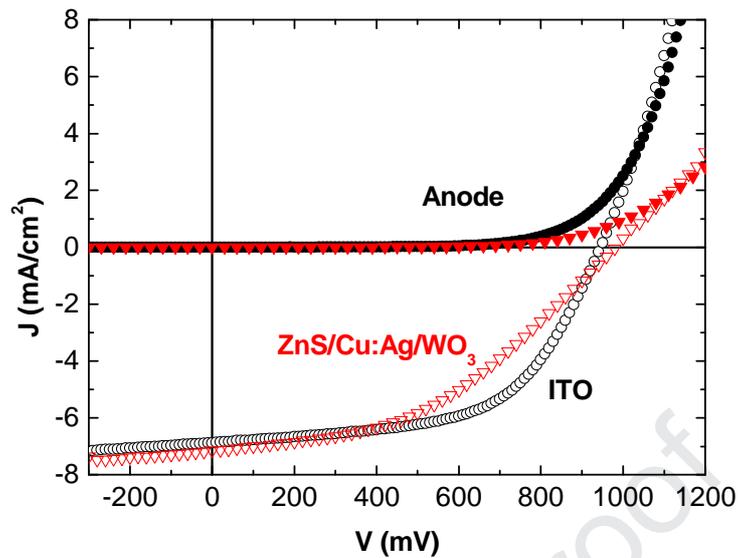
14

Figure 11: J-V characteristics of classical OPVs (Anode/MoO$_3$/CuI/SubPc/C$_{60}$/BCP/Al) with ZnS/Cu:Ag/Ag/WO$_3$(▼) or ITO (■). The curve with full symbol was obtained in the dark that with open symbol under AM1.5 illumination.

Anode	Voc (V)	Jsc (mA/cm^2)	FF (%)	η (%)	Rs (Ω)	Rsh (Ω)
ITO	0.94	6.80	57.5	3.63	32	1020
ZnS/Cu:Ag/Ag/WO$_3$	0.98	7,14	43	3.02	73	815

Table 5: Comparison of the parameters of the OPVs with ZnS/Cu:Ag/Ag/WO$_3$ or ITO as anode.

Promising results were obtained even if ITO gives higher OPVs efficiency. It can be seen in Table 5 that nearly similar Voc are obtained, while Jsc of OPV using ZnS/Ag/WO$_3$ as anode is higher than that of classical OPVs using ITO. Nevertheless, FF is significantly smaller which results in smaller efficiencies for OPCs using the new electrode. Since the roughness of the ZCAW electrodes is of the same order than that of ITO, around one nanometer, it is necessary to look for another explanation. Actually, as in the case of ZAT TCE, there is some metal present on the surface of the ZCAW electrode, here Cu, which may explain the small FF value. This negative effect is visible in Table 5 through the series resistance Rs and shunt resistance Rsh values. The Rs value, 73 Ω is large, while that of Rsh, 815 Ω is quite small. The large value of Rs can be attributed to a poor band matching at the interface anode/SubPc. Actually, the work function of Cu being around 4.7 eV while the Highest Occupied Molecular Orbital of SubPc is 5.6 eV, which induces a bad band matching at the interface anode/SubPc and a small FF value. Therefore this poor band matching increases Rs, which penalizes the OPVs performances. On the other hand, the high ability of Cu to diffuse makes it possible for leak paths to appear through the thin organic layer, inducing a quite high saturation current and a small Rsh.

4. Conclusions / Perspectives

New TCEs based on D/M/D structures are very stable when Ag is the metal while it is not with Cu. Here, we show that the substitution of Cu:Ag alloy to pure Cu improves significantly the stability of the structures. The best results are obtained with WO_3 (45 nm)/Cu:Ag (**16 nm**)/Ag (1 nm)/WO_3 (20 nm) multilayer structures. Its maximum transmission is 85.2 % and its sheet resistance is 31 Ω/sq. When they are used as anode in OPCs, these new electrodes allow achieving performances of the same order of magnitude than those obtained with ITO. The smaller value of FF is attributed to the presence of a small concentration of Cu atoms present at the interface TCE/organic material. Nevertheless, the obtained results with the Cu:Ag alloy confirm that $ZnS/Cu:Ag/Ag/WO_3$ structures open new promising perspectives for using Cu in D/M/D TCE. These results are clearly better than those obtained with Cu:Ni or Cu:Al alloys, even if the presence of Cu traces at the surface of the TCE still limits hole collection. Surprisingly, similar difficulty is encountered in the case of $ZnS/Ag/TiO_2$ structures. Here, Ag is present on the electrode surface which limits significantly their performances. In the future, it will be necessary to avoid the presence of metal at the surface of the structure either by increasing the thickness of the dielectric film or by covering the metal film with a diffusion barrier such as Cr, W or Ni.

Acknowledgements

16

References

1. M.C. Scharber, N.S. Sariciftci, Efficiency of bulk-heterojunction organic solar cells, Progress in Polymer Science 38 (2013) 1929-1940.

2. J. C. Bernède, Organic photovoltaic cells:History, principle and techniques, Journal of the Chilean Chemical Society 53 (2008) 1549-1564.

3. T. Minami, Substitution of transparent conducting oxide thin films for indium tin oxide transparent electrode applications, Thin Solid Films 516 (2008) 1314-1321.

4. W. Cao, J. Li, H. Chen, J. Xue, Transparent electrodes for organic optoelectronic devices: a review, J. Photoni. Energy 4 (2014) 040990-040991-28.

5. H. Lu, X. Ren, D. Ouyang, and W. C. H. Choy, Emerging Novel Metal Electrodes for Photovoltaic Applications, Small 2018, 1703140, DOI: 10.1002/smll.201703140.

6. C. Guillén, J. Herrero, TCO/metal/TCO structures for energy and flexible electronics,Thin Solid Films 520 (2011) 1-17.

7. L. Cattin, J.C. Bernède, M. Morsli, Toward indium-free optoelectronic devices: Dielectric/Metal/Dielectric alternative conductive transparent electrode in organic photovoltaic cells, Phys. Status Solidi A 210 (2013) 1047-1061.

8- J. C. Bernède, L. Cattin, Dielectric/Metal/Dielectric flexible transparent electrodes, from smart window to semi-transparent solar cells, Asian Journal of Engineering and Technology 7 (2019) DOI: https://doi.org/10.24203/ajet.v7i3.5710

9. R. R. Søndergaard, M. Hôsel, F. C. Krebs, Roll-to-Roll fabrication of large area functional organic materials, J. Polymer Science B: Polymer Phys. 51 (2013) 16-34.

10. https://www.heliatek.com/en/press/press-releases/details/worlds-largest-facade-installed-with-organic-photovoltaics-in-the-port-of-duisburg 10.

11. I. Péréz Lopéz, L. Cattin, D.-T. Nguyen, M. Morsli, J.C. Bern_ede, Dielectric/Metal/Dielectric structures using Copper as metal and MoO_3 as dielectric for use as transparent electrode, Thin Solid Films 520 (2012) 6419-6423.

12. S. Tuo, L. Cattin, H. Essaidi, L. Peres, G. Louarn, Z. El Jouad, M. Hssein, S. Touihri, S.Yapi Abbe, P. Torchio, M. Addou, J.C. Bernède, Stabilisation of the electrical and optical properties of dielectric/Cu/dielectric structures through the use of efficient dielectric and Cu:Ni alloy, Journal of Alloys and Compounds 729 (2017) 109-116.

13. D.-E. Rabia, M. Blais, H. Essaidi, N. Stephant, G. Louarn, M. Morsli, S. Touihri, J.C. Bernède, L. Cattin, Stabilisation of Cu films in WO_3/Ag/Cu:Al/WO_3 structures through their doping by Al and Ag, Thin Solid Films 669 (2019) 613–619

14. L. Cattin, Y. Lare, M. Makha, M. Fleury, F. Chandezon, T. Abachi, M. Morsli, K. Napo, M. Addou, J.C. Bernède, Effect of the Ag deposition rate on the properties of conductive transparent MoO_3/Ag/MoO_3 multilayers, Sol. Energy Mater. Sol. Cell. 117 (2013) 103-109.

15. G. Haacke, New figure of merit for transparent conductors, J. Appl. Phys. 47(1976) 4086-4089.

16. M. Hssein, S. Tuo, S. Benayoun, L. Cattin, M. Morsli, Y. Mouchaal, M. Addou, A. Khelil, J.C. Bernède, Cu-Ag bi-layer films in dielectric/metal/dielectric transparent electrodes as ITO free electrode in organic photovoltaic devices, Org. Electron. 42 (2017) 173-180.

17. Y. Berredjem, N. Karst, L. Cattin, A. Lkhdar-Toumi, A. Godoy, G. Soto, F. Diaz, M.A. del Valle, M. Morsli, A. Drici, A. Boulmokh; A.H. Gheid, A. Khelil, J.C. Bernède, Plastic

photovoltaic cells encapsulation, effect on the open circuit voltage,Dyes and Pigments 78 (2008) 148-156.

18. L. Cattin, J.C. Bernède, Y. Lare, S. Dabos-Seignon, N. Stephant, M. Morsli, P.P. Zamora, F.R. Diaz, M.A. del Valle, Improved performance of organic solar cells by growth optimization of MoO3/CuI double-anode buffer, Phys. Status Solidi A 210 (2013) 802-808.

19.T. Abachi, L. Cattin, G. Louarn, Y. Lare, A. Bou, M. Makha, P. Torchio, M. Fleury, M. Morsli, M. Addou, J. C. Bernède, Highly flexible, conductive and transparent MoO_3/Ag/MoO_3 multilayer electrode for organic photovoltaic cells. Thin Solid Films 545 (2013) 438-444.

20. A. Bou, Ph. Torchio, S. Vedraine, D. Barakel, B. Lucas, J.C. Bernède, P.Y. Thoulon, M. Ricci, Numerical optimization of multilayer electrodes without indium for use in organic solar cells, Sol. Energy Mater. Sol. Cell. 125 (2014) 310-317.

21. A. Bou, Ph. Torchio, D. Barakel, P.Y. Thoulon, M. Ricci, Numerical-experimental coupled study of TiOx/Ag/TiOx as transparent and conductive electrode, Thin Solid Films 617 (2016) 86-94.

22 A. Bou, P. Torchio, D. Barakel, F. Thierry, A. Sangar, P.Y. Thoulon, and M. Ricci, "Indium Tin Oxide-free Transparent and Conductive Electrode based on SnOx|Ag|SnOx for Organic Solar Cells",Journal of Applied Physics, Vol. 116, No. 2, 023105 (2014).

23. L. Peres, A. Bou, D. Barakel, P. Torchio, ZnS|Ag|TiO2 multilayer electrodes with broadband transparency for thin film solar cells, RSC Advances 6 (2016) 461057-61063.

24. A. Bou, M. Chalh, S. Vedraine, B. Lucas, D. Barakel, L. Peres, P.Y. Thoulon, M. Ricci, and Ph. Torchio, Optical role of the thin metal layer in a TiOx/Ag/TiOx transparent and conductive electrode for organic solar cells, RSC Advances, 6 (2016) 108034–108044.

25. L. Cattin, El Jouad, N. Stephant, G. Louarn, M. Morsli, M. Hssein, Y. Mouchaal, S. Thouiri,M. Addou, A. Kheli, J. C. Bernède, Dielectric/Metal/Dielectric alternative transparent electrode: Observations on stability/degradation, Journal of Physics D: Applied Physics 50 (2017) 375502 (13pp).

26. H. Chen, J-M. Zuo, Structure separation of Ag-Cu alloy thin films, Acta Materialia 55 (2007) 1617-1628.

27. Y. Mouchaal, G. Louarn, A. Khelil, M. Morsli, N. Stephant, A. Bou, T. Abachi, L. Cattin, M. Makha, P. Torchio, J.C. Bernède, Broadening of the transmission range of dielectric/metal multilayer structures by using different metals, Vacuum 111 (2015) 32-41.

28. Z. El Jouad, M. Morsli, G. Louarn, L. Cattin, M. Addou, J. C. Bernède, Improving the efficiency of subphthalocyanine based planar organic solar cells through the use of MoO_3/CuI double anode buffer layer.Solar Energy Materials & Solar Cells 141 (2015) 429-435.

29. Z. el Jouad, L. Barkat, N. Stephant, L. Cattin, N. Hamzaoui, A. Khelil, M. Ghamnia, M. Addou, M. Morsli, S. Béchu, C. Cabanetos, M. Richard-Plouet, P. Blanchard, J.C. Bernède, Ca/Alq_3 hybrid cathode buffer layer for the optimization of organic solar cells based on a planar heterojunction. J. Phys Chem Solids 98 (2016) 128-135.

30. H-W Lu, C-W. Huang, P-C. Kao, S-Y. Chu, ITO-free organic light-emitting diodes with MoO_3/Al/MoO_3 as semitransparent anode fabricated using thermal deposition method, Appl. Surf. Science 347 (2015) 116-121.

[31] J.C. BERNEDE. Polarized Memory Switching in M.I.S. Thin Films Structure".
Thin Solid Films. Vol. 81, n°2 (1981), p. 155-160.

Figures

Figure 1: Comparison between simulated and measured values of transmittance (T), reflectance (R) and absorbance (A) for a ZnS (35 nm) / Ag (10 nm) / TiO_2 (25 nm) electrode.

Figure 2: Evolution with time of the sheet resistance of WO_3/Cu:Ni/WO_3 (▲), WO_3/Cu:Al/Ag/WO_3 (●) and ZnS/Cu:Ag/Ag/WO_3 (■) structures.

Figure 3: Variation of the light transmission of the structures

ZnS (45 nm)/ Cu:Ag x nm)/ Ag (1 nm)/WO_3 (20 nm)

with different thicknesses for the Cu:Ag layer.

Figure 4: a: Surface visualization of a ZnS(45 nm)/ Cu:Al 16 nm)/ Ag (1 nm)/WO_3 (20 nm) multilayer structure; inset: same film at higher magnification.

　　　b- Cross section visualization in the backscattering mode of a ZnS(45 nm)/ Cu:Ag (16 nm)/ Ag (1 nm)/WO_3 (20 nm) structure.

Figure 5: AFM image of the surface of a ZnS(45 nm)/ Cu:Al 16 nm)/ Ag (1 nm)/WO_3 (20 nm) multilayer structure.

Figure 6: Figure 6: XPS profiles of Glass/ZnS (45 nm)/Cu:Ag (16 nm)/Ag (1 nm)/WO_3 (20 nm) and typical structural diagram of a structure.

Figure 7: J-V characteristics of inverted OPVs (Cathode/BCP/C_{60}/SubPc/MoO_3/Al) with ZnS/Ag/TiO_2(□) or ITO (▲) as cathode.

Figure 8: AFM image of the surface of ZnS/Ag/TiO_2.

Figure 9: J-V characteristics of classical OPVs (Anode/MoO_3/SubPc/C_{60}/BCP/Al) with ITO (□) or ZnS/Ag/TiO_2 (○) as anode

Figure 10: Figure 10: XPS survey spectrum of a ZnS/Ag/TiO2 structure.

Figure 11: J-V characteristics of classical OPVs (Anode/MoO_3/CuI/SubPc/C_{60}/BCP/Al) with ZnS/Cu:Ag/Ag/WO_3(▼) or ITO (■). The curve with full symbol was obtained in the dark that with open symbol under AM1.5 illumination.

Tables

Table 1: Variation of the main parameters of the ZnS (45 nm)/ Cu:Al (x nm)/Ag (1 nm)/WO_3 (20 nm) multilayer structures with the thickness of Cu:Al layer, the Ag layer thickness being fixed at 1 nm.

Table 2: Variation of the main parameters of the ZnS (45 nm)/Cu:Ag (x nm)/Ag (y nm)/WO_3 (20 nm) multilayer structures, y, the Ag thickness and x the Cu:Ag thickness being used as parameters, while the sum x+y is constant: 17 nm.

Table 3: Resistance evolution after outer bending and inner bending as a function of the number of bending cycles for PET/ ZnS(40 nm)/ Cu:Al 16 nm)/ Ag (1 nm)/WO_3 (35 nm) and PET/ITO structures.

Table 4: Comparison of the parameters of the OPVs with ZnS/Ag/TiO_2or ITO as cathode.

Table 5: Comparison of the parameters of the OPVs with ZnS/Cu:Ag/Ag/WO_3or ITO as anode.

19

Highlight:

- ZnS/Ag/TiO2 and ZnS/Metal/WO3 can be used as transparent conducive electrode

-Cu :Ag (5at.%) alloy stabilizes properties of ZnS/Metal/WO3 structures.

-ZnS/Ag/TiO2 modeling permits to estimate the optimum thickness of the different layers

-Organic solar cells using these ITO free electrodes achieve promising performances.

Dear Editor,
We would like to submit for publication in your review Journal of Alloys and Compounds the manuscript entitled (new title):
"**New Dielectric/Metal/Dielectric electrode for organic photovoltaic cells using Cu:Al alloy as metal."**

By L. Cattin, A. El Mahlali, M. A. Cherif, S. Touihri, Z. El Jouad. Y. Mouchaal, P. Blanchard, G. Louarn, H. Essaidi, M. Addou, A. Khelil, P. Torchio and JC Bernède.

The manuscript has been corrected in the light of the comments of the reviewers. We thank them for their help in improving our manuscript;

We confirm that:
1. The article is original and has not be submitted to other review.
2. The article has been written by the stated authors who are all aware of its content and approve its submission to Journal of Alloys and Compounds.

Sincerely yours

J C Bernède
Corresponding author

E-mail jean-christian.bernede@univ-nantes.fr